RSC Publishing Nanoscale

Controllability of the Coulomb charging energy in close-packed nanoparticle arrays

Journal:	*Nanoscale*
Manuscript ID:	NR-ART-05-2013-002334.R1
Article Type:	Paper
Date Submitted by the Author:	25-Jun-2013
Complete List of Authors:	Duan, Chao; Peking University, Department of Electronics Wang, Ying; Peking University, Department of Electronics Sun, Jinling; Peking University, Department of Electronics Guan, Changrong; Peking University, Department of Electronics Grunder, Sergio; University of Basel, Department of Chemistry Mayor, Marcel; University of Basel, Department of Chemistry Peng, Lian-Mao; Peking University, Electronics Liao, Jianhui; Peking University, Department of Electronics

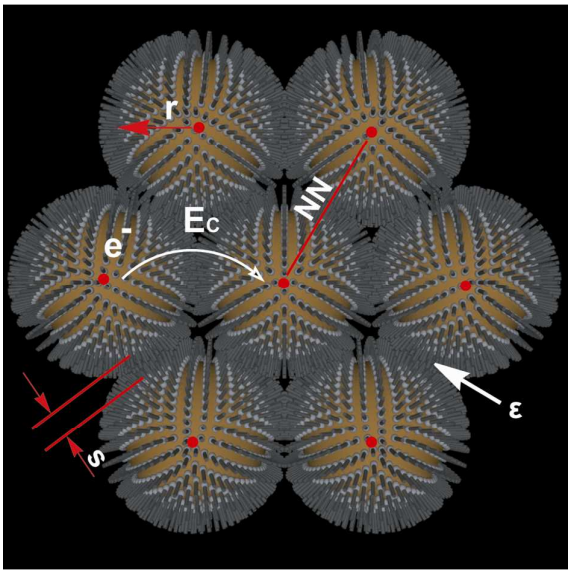

The controllability of the Coulomb charging energy in nanoparticle arrays has been systematically and comprehensively studied by tuning various parameters, i.e., the nanoparticle core size, the nearest neighbor number, the inter-particle distance, and the dielectric constant of ligands.

Controllability of the Coulomb charging energy in close-packed nanoparticle arrays

Chao Duan,[1] Ying Wang,[1] Jinling Sun,[1] Changrong Guan,[1] Sergio Grunder,[2] Marcel Mayor,[2,3] Lianmao Peng,[1] and Jianhui Liao[1,*]

[1]*Key Laboratory for the Physics and Chemistry of Nanodevices, Department of Electronics, Peking University, Beijing 100871, China*

[2]*University of Basel, Department of Chemistry, St. Johannsring 19, CH-4056 Basel, Switzerland*

[3]*Karlsruhe Institute of Technology, Institute of Nanotechnology, P.O.Box 3640, D-76021 Karlsruhe, Germany*

(Dated: August 10, 2013)

Abstract

We studied the electronic transport properties of metal nanoparticle arrays, particularly focused on the Coulomb charing energy. By comparison, we confirmed that it is more reasonable to estimate the Coulomb charging energy using the activation energy from the temperature-dependent zero-voltage conductance. Based on this, we systematically and comprehensively investigated the parameters that could be used to tune the Coulomb charing energy in nanoparticle arrays. We found that four parameters, including the particle core size, the inter-particle distance, the nearest neighboring number, and the dielectric constant of ligand molecules, could significantly tune the Coulomb charing energy.

*Electronic address: Jianhui.Liao@pku.edu.cn

Nanometer-sized metal particles, often called nanoparticles, have attracted more and more research attention in the last two decades, mainly due to their size-dependent properties in electronics [1], optics [2], and magnetics [3]. These nanoparticles not only provide ideal model systems to discover and understand novel physical phenomena in small structures [4], but also exhibit exciting potential in electronic and optoelectronic devices [5].

Nanoparticles can be arranged into one-dimensional (1D) [6], two-dimensional (2D) [7], and three-dimensional (3D) [8] superlattices, just like the structures made from natural atoms. Due to this analogy, nanoparticles are often called "artificial atoms", and the assemblies made from them are called "artificial solids". More interestingly, the properties of artificial solids are determined not only by individual nanoparticles, but also by the coupling between them [9, 10]. At least two reasons have urged the research in the field of nanoparticles to turn from individual nanoparticles to nanoparticle assemblies. One is that nanoparticle assemblies have exhibited more and more interesting collective properties because of the interactions between components [11, 12]. The other is that nanoparticle assemblies are much easier to be handled for device applications.

In nanoparticle assemblies, the Coulomb charging energy is one of the most important energy scales and parameters [13]. The Coulomb charging energy of an isolated nanoparticle is defined as the energy needed to add an extra electron onto an electronically neutral nanoparticle. In nanoparticle assemblies, it is determined by more parameters, therefore is more complex [14]. Although many research efforts have been devoted to investigate the Coulomb charging energy in nanoparticle assemblies [15–30], discrepancies still exist about some fundamental questions. One example is about the estimation of the Coulomb charging energy in nanoparticle assemblies. The values for the same system obtained by different methods and models can be remarkably distinctive. One more example is about the relationship between the Coulomb charging energy and the inter-particle distance. Some papers show that the Coulomb charging energy in nanoparticle assemblies depends on the inter-particle distance [16, 17], while other paper shows that the influence of the inter-particle distance can be ignored provided the diameter of particles is smaller than one micrometer [18]. Although it is well known that the Coulomb charging energy of nanoparticle arrays can be tuned by changing the diameter of particles, more approaches are still required to change the Coulomb charging energy to increase its controllability. For example, once devices made from nanoparticle arrays are done, it is not easy to change the diameter of nanoparticles any longer. In these cases, we need other methods to tune the Coulomb charging energy of the devices if required. However, studies on the dependence of the Coulomb charging energy upon different

parameters often focused on one or two parameters [15, 16, 19, 29, 30]. Therefore, the tuning of the Coulomb charging energy with different methods is critical not only for understanding the charge transport process in nanoparticle assemblies, but also for device applications of artificial solids. In this paper, we measured the electronic transport properties of devices made from spatially well-defined close-packed nanoparticle arrays at different temperatures. Various parameters were systematically tuned to investigate the relationship between them and the Coulomb charging energy of corresponding nanoparticle arrays.

The Au nanoparticles used in this paper were synthesized using the wet chemical method. The detailed process can be found somewhere else [31]. In brief, the tetrachloroauric acid was reduced by trisodium citrate and tannic acid, forming Au nanoparticles in water solution. Adding different amount of tannic acid results in Au nanoparticles with different diameters. We controlled the diameter of the synthesized nanoparticles in the range from 5 nm to 25 nm. Alkanethiols were used to encapsulate gold nanoparticles. Then, these alkanethiol-capped gold nanoparticles were dispersed in chloroform.

Two-dimensional nanoparticle arrays were prepared by self-assembly at the air/water interface. Figure 1 shows transmission electron microscope (TEM) images of close-packed nanoparticle arrays made from octanethiol-capped Au nanoparticles. Here, arrays with only three different core sizes are presented, i.e., 6.66 nm (Fig. 1a), 10.02 nm (Fig. 1b), and 21.35 nm (Fig. 1c). From these TEM images, the nanoparticle arrays show three specialities. Firstly, the nanoparticles synthesized with our method have good monodispersity. The measured standard diversity of nanoparticle with each size is smaller than 10%. Secondly, nanoparticles are in hexagonal close-packed arrays order, regardless of core sizes. Thirdly, neighboring nanoparticles are well separated from each other by ligand molecules, i.e., the insulating alkanethiols, which act as tunneling barriers for charge transport. To illustrate all of the parameters that we can tune in a nanoparticle array, we draw a schematic unit cell of a nanoparticle array, as shown in Fig. 1d. The parameters associated with the Coulomb charging energy in a nanoparticle array include the nanoparticle radium **r**, the inter-particle distance **s**, the nearest neighbor number **NNN**, and the dielectric constant of the surrounding environment ε. A systematical and comprehensive study on the influence of the Coulomb charging energy by these parameters will be presented in the following.

Devices measured in this work were fabricated by the combination of lithographic techniques with the self-assembly method. The detailed procedures can be found in our previous paper [32]. Figure 2a shows the schematic of a nanoparticle device. The regions of electrodes and the channel

were made protuberant so that only these regions could be covered with nanoparticle arrays when the micro-contact printing was used to transfer 2D nanoparticle arrays from the water surface. Our fabrication method has several advantages. Firstly, the shape and size of the nanoparticle arrays under test are well-controlled. Every step in the process of fabrication is separated. We could make the overall shape of the nanoparticle arrays between electrodes be the same, which makes the comparison between different devices more reasonable. Secondly, our method ensured good electrical contact between the nanoparticle arrays and the electrodes. In the fabrication, we controlled the thickness of the electrodes to be thinner than 30 nm, which is very close to the diameter of an individual nanoparticle. All of our measurements confirmed that the electric connection between the electrodes and the nanoparticle arrays under test could be guaranteed.

Figure 2b shows a SEM image of one typical device. The nanoparticle array between two electrodes is rectangular. It is about 2 μm long and 60 μm wide. The large aspect ratio is to make the array measurable at low temperatures, because nanoparticle arrays with alkanethiol ligands are very insulating, especially for long alkanethiol molecules. The inset in Fig. 2b shows a high magnification SEM image of the nanoparticle array between electrodes. The hexagonal close-packed ordering of the array can be distinguished. This is another advantage of our fabrication method: to maintain the internal order while controlling the overall shape of the nanoparticle arrays.

To investigate the electronic transport properties of devices, a cryostat was used to lower the temperature of samples. The current-voltage curves were measured at different temperatures for each device. Figure 2c shows typical current-voltage curves of a device made from octanethiol-capped 10 nm nanoparticles at temperatures ranging from 5 K to 300 K. These curves present general characters of all devices we measured. Firstly, the curves get more and more non-linear with decreasing temperature. Secondly, the zero-voltage conductance has a positive temperature coefficient. This is a remarkable attribute of an insulator, which indicates that the nanoparticle array is very resistive. Thirdly, the current starts to be suppressed at low temperature in the low voltage region. The appearance of the threshold voltage in the current-voltage curves is normally considered to be the consequence of the Coulomb blockade. These characters are consistent with other measurements on nanoparticle arrays [15, 26–28, 33, 34].

We first focused on the dependence of the Coulomb charging energy on the nanoparticle core size. However, before this, we should choose a reasonable method to estimate the Coulomb charging energy. In published papers, there exist four different methods or models to estimate the

Coulomb charging energy of nanoparticle arrays. The first one applies the simplest model, using the formula for an isolated nanoparticle to the case of nanoparticle arrays [23]. In this model, the Coulomb charging energy is expressed as

$$E_{C1} \approx \frac{e^2}{4\pi\varepsilon D}$$

where D is the diameter of the nanoparticles and ε is the dielectric constant of the surrounding environment. This model only takes into account the self-capacitance of the nanoparticles and ignores the capacitance between neighboring nanoparticles. Therefore, the value of the Coulomb charging energy obtained from this model is supposed to be overestimated. The second model that were more widely used assumes a metal nanoparticle surrounded by a layer of dielectric material with the thickness s and another infinite concentric metal layer [15, 20, 22, 27, 28]. The Coulomb charging energy calculated from this model follows the equation

$$E_{C2} \approx \frac{e^2}{4\pi\epsilon}(\frac{1}{D} - \frac{1}{D+s})$$

This model apparently exaggerates the contribution of the mutual capacitance between neighboring nanoparticles. It is expected that the value of the Coulomb charging energy deduced from this model is underestimated. The third method to estimate the Coulomb charging energy of nanoparticle arrays is from the measured threshold voltage at low temperatures [33]. The threshold voltage of a nanoparticle array means the smallest voltage that should be applied to overcome the upward potential in the first path connecting the source and drain electrodes. Experimental and theoretical studies found that the threshold voltage is linear with the temperature [33, 34]. The threshold voltage at 0 K $V_T(0)$ can be obtained from the measured V_T at finite temperatures. To extract the threshold voltages from current-voltage curves at finite temperatures, we used the method described below. Suppose the relationship between the current and the voltage obeys the scaling law, $I \propto (\frac{V}{V_{Th}} - 1)^{\varsigma}$, where V_T is the threshold voltage, ς the scaling exponent. Then, $\frac{I}{dI/dV} \propto (V - V_T)/\varsigma$. The V_T and ς can be obtained by linear fitting. Taking into account the array geometry, the Coulomb charging energy can be calculated from the threshold voltage $V_T(0)$ using the following formula

$$E_{C3} \approx \frac{eV_T(0)}{\alpha N}$$

where α is a prefactor to account the percentage of rising energy steps in the first current path connecting two electrodes for a provided array geometry and N is the number of particles in the first current path. Normally, N is taken as the number in a straight path without considering

the meandering of the actual current path. From this point of view, the value of the Coulomb charging energy got from this model should be a little overestimated. The fourth method takes advantage of a simple thermally activated transport theory [36], which predicts that the zero-voltage conductance follows the Arrhenius equation

$$G_{V=0} \propto exp(-\frac{E_a}{k_B T})$$

whre E_a is the activation energy and k_B is the Boltzmann constant. When the thermal energy is smaller than the Coulomb charging energy, the activation energy can be considered as the same to the Coulomb charging energy.

We measured the electronic transport properties of devices made from nanoparticle arrays with different metal core sizes but with the same ligand molecule. We obtained the zero-voltage conductance of each device at a specific temperature by linear fitting the current-voltage curve at small bias ranging from -0.3 V to 0.3 V. Considering the large distance between electrodes and small diameter of nanoparticles, the current-voltage curves are safely in the linear range according to the nonresonance tunneling theory. Our measured current-voltage curves are indeed linear at small bias. The zero-voltage conductance for each sample was plotted as a function of the inverse temperature, as shown in Fig. 3a. As shown in Fig. 2c, at low temperature, the current is suppressed when the bias is smaller than a voltage threshold, which makes the zero-voltage conductance immeasurable. On the other hand, when the temperature is just above the critical temperature, the current is too low to measure. For reliable measurement of the zero-voltage conductance, we show the data about 50 K. In the temperature range from 50 K to 250 K, the linear relationship between the zero-voltage conductance and the inverse temperature in a semi-log scale strongly indicates the thermally activated model for our devices. For comparison, we calculated the Coulomb charging energy obtained from four different methods for different metal core sizes. As shown in Fig. 3b, results from all methods exhibit the same tendency that the Coulomb charging energy increases with decreasing nanoparticle diameter. Interestingly, the values calculated from the first model are the largest for each size, while the values from the second model are the smallest. This result is consistent with our analysis given above that the first model is overestimated and the second model is underestimated. More importantly, the values from the third model are bigger than that from the fourth model. As we mentioned, the third model is supposed to be a little overestimated. Therefore, it is more reasonable to take the values obtained from the fourth method as the Coulomb charging energy of nanoparticle arrays.

The inter-particle distance is another parameter that might be used to tune the Coulomb charging energy in nanoparticle arrays. Although some simulation shows that the inter-particle distance does not contribute to the Coulomb charging energy significantly provided the particle size is smaller than 1 μm [18], some measurements have demonstrated that it is not the case [16, 17]. Here, we used nanoparticles from the same batch to prepare devices, which ensured the same core size. Four kinds of alkanethiol molecules with different carbon atoms were used to serve as ligands. The number of carbon atoms in alkanethiols changes from 4 to 10. The molecular structures of these four alknaethiols are shown in Fig. 4a. For nanoparticle arrays with each kind of alkanethiol, we measured several devices. Figure 4b shows the typical zero-voltage conductance curves as a function of inverse temperature for each alkanethiol-capped nanoparticle array. The curves show that the shorter the ligand molecules, the higher the conductance of the arrays. This can be understood from the tunneling mechanism, which predicts that the current is exponentially sensitive to the inter-particle distance. As we change the length of the ligand molecules, we essentially change the inter-particle distance in the arrays, as confirmed in Fig. 4c. One can also see that the linear dependence of the zero-voltage conductance upon the inverse temperature in a semi-log scale holds for all different ligand molecules. This enables us to extract the Coulomb charging energy for arrays with different inter-particle distances, as shown in Fig. 4c. In our experiments, we determined the interparticle distance by two procedures. First, the average diameter of nanoparticles D was determined using TEM images of nanoparticles. Second, SEM images of measured devices were used to measure the center-center distance L between the first and eleventh nanoparticles aligned in a line in the array, which equals to 10 times of D+s, where D is the diameter of nanoparticles and s is the interparticle distance. It is reasonable to obtain the average interparticle distance in this way. Our experimental result shows that the Coulomb charging energy in nanoparticle arrays indeed depends on the inter-particle distance. Increasing the inter-particle distance leads to the increase of the Coulomb-charging energy. Qualitatively, we can explain this behavior by using a simple model [35]. This model estimates the pairwise capacitance between two neighboring nanoparticles with the following formula:

$$C_{nn} \sim Dln(1 + D/s)$$

where D is the nanoparticle diameter and s is the inter-particle distance. This model predicts that the mutual capacitance between two neighboring nanoparticles decreases with increasing the inter-particle distance, provided the nanoparticle diameter maintains the same. The decrease of

the mutual capacitance results in the increase of the Coulomb charging energy, which is consistent with our experimental results. We also note that there is a discrepancy between the data and the proposed equation in detail, although the global trend is consistent. We attribute the discrepancy between the model and the data to the uncontrolled interparticle distance between different layers during device preparation. The model only considers the change of the charging energy due to the change of the nearest neighbor number. But when we printed more layers on the device, we could not guarantee that the interparticle distance of each layer was exactly the same. This might be the reason resulting in the discrepancy between the model and the data.

Another important parameter in nanoparticle ensembles is the nearest-neighboring-number (NNN). However, this parameter has seldom been tuned so far, mainly because of the difficulty of experimental implementation [30]. In our device preparation procedure, we could easily change the dimensionality of the nanoparticle arrays under test from 2D to 3D by increasing the array thickness layer by layer. In this way, we could increase the NNN of individual nanoparticles in the arrays. Figure 5a shows the schematic of printing an excess layer of nanoparticle array onto a device with two layers. We started from a device with one layer of nanoparticle array. After measuring the electronic transport properties, we printed another layer of nanoparticle array onto the same device and measured the electronic transport properties again, and so on. Our method guarantees that every newly printed nanoparticle layer is exactly on top of the previous array and has the same size and shape.

Figure 5b shows the zero-voltage conductance as a function of the inverse temperature for the same device with different layers of nanoparticle array. The diameter of nanoparticles was 10 nm and the ligand was octanethiol. The data show that the zero-voltage conductance increases as the number of nanoparticle layer increases. This is reasonable because devices with more nanoparticle layers can provide more current paths. The Coulomb charging energy for the device with different number of nanoparticle layers extracted from the temperature-dependent zero-voltage conductance is shown in Fig. 5c. Interestingly, the value of the charging energy decreases rapidly for the first few layers, then starts to level off for more layers. We can explain this behavior by using a simple model. The total capacitance of an individual nanoparticle can be written as $C = C_{self} + C_{mutual}$, where C_{self} is the self capacitance of an individual nanoparticle and C_{mutual} is the total mutual capacitance between this nanoparticle and the surrounded neighboring nanoparticles. For a hexagonal close-packed nanoparticle monolayer, the average NNN is 6. Assume the pairwise capacitance between two neighboring nanoparticles is C_{nn}, for monolayer, $C_{mutual} = 6C_{nn}$. For

bilayer, the NNN number of each nanoparticle is increased to 9. Therefore, the total capacitance is $C = C_{self} + 9C_{nn}$. For trilayer nanoparticle arrays, the NNN number for nanoparticles in the upper or lower layer is still 9, but 12 for the middle layer. Then, the average total capacitance is $C = C_{self} + \frac{2*9C_{nn}}{3} + \frac{12C_{nn}}{3}$, and so on. This simple calculation also predicts the fast decrease of the Coulomb charging energy for the first few layers and level off for more layers, which is consistent with our experimental data.

The fourth parameter that we studied to tune the Coulomb charging energy of nanoparticle arrays is the dielectric constant of the surrounding molecules. In the as-prepared nanoparticle arrays, the nanoparticles were capped by alkanethiols. To change the molecules surrounding nanoparticles, we used the molecular exchange method to partially displace alkanethiols by dithiolated oligo(phenylene ethynylene)(OPE) molecules [37, 38]. The molecular structures of octanethiol and OPE dithiol are presented in Fig. 6a. It is clear that the octanethiol molecule is saturated while the OPE molecule is conjugated.

For molecular exchange, the as-prepared nanoparticle arrays were immersed in 1mM solution of OPE molecules for more than 12 hours. The electronic transport properties of the same nanoparticle arrays were measured before and after molecular exchange. Figure 6b shows the zero-voltage conductance as a function of the inverse temperature for three devices measured before and after molecular exchange. The average charging energy before and after molecular exchange is 8.05±0.87 meV and 5.57±0.92 meV, respectively. The dielectric constant of alkanes are typically in the range between 1.9-2.2 [39, 40], and 3.1-3.9 for OPE molecules [41, 42]. In previous literature, Bernard et al. has investigated the molecular exchange in nanoparticle arrays using spectroscopy techniques. It was found that only 20%-40% of the surface area of nanoparticle was occupied by OPE molecules after molecular exchange [43]. We believe that it holds true also for our case because of the similar experimental conditions, which indicates that the dielectric constant after molecular exchange might be smaller than that of the pure OPE molecules. We take the dielectric constant for mixed molecules with 20%-40% OPE molecules, giving rise to the value in the range from 2.14 to 2.88 after molecular exchange. The ratio of the dielectric constant before exchange to that after exchange is in the range from 0.65 to 1.03. According to our measurements, the ratio of the measured charging energy is 0.65±0.2, which is in the range of the ratio of the two dielectric constants. Our results confirmed that the molecules with different dielectric constants could also be used to tune the Coulomb charging energy of nanoparticle arrays.

In summary, we obtained two conclusions through systematically studies of the charge transport

properties of close-packed nanoparticle arrays. First, it is more reasonable to estimate the Coulomb charging energy of nanoparticle arrays from the Arrhenius fitting of the temperature-dependent zero-voltage conductance. Second, the Coulomb charging energy of nanoparticle arrays can be effectively tuned by various parameters associated with the capacitance of nanoparticles. The controllability of the Coulomb charging energy of nanoparticle arrays suggested by our results will provide more approaches towards desired nanoparticle arrays for fundamental studies as well as device applications.

Methods

Preparation of Au nanoparticles and self-assembly of two-dimensional nanoparticle arrays

Alkanethiol-capped gold nanoparticles with different diameters were prepared and dispersed in chloroform according to the method described in the literature [31]. The self-assembly process was performed in a fume hood. A Teflon beaker was used as a container to produce the slightly convex water surface. Typically, ~400 μl nanoparticle solution was cast onto the water surface. After 10-15 minutes, the solvent evaporated, leading to the formation of ordered 2D naoparticle arrays.

Fabrication of PDMS stamps and transfer of nanoparticle arrays

Flat PDMS Stamps were prepared using clean silicon chips as masters. The silicon wafers were thoroughly cleaned by ultrasonic treatment in pure water, acetone, and isopropanol, respectively. Then, the mixture of a prepolymer gel and a curing agent (Sylgard 184, Corning) was cast on the silicon surface. After degassing at room temperature for 1 hour, the mixture was baked at 60°C for 1-2 hours. Afterward, the PDMS was peeled off the master and cut into desired shape.

The Langmuir-Schaefer technique was used to transfer nanoparticle arrays from the water surface onto solid substrates. Briefly, a PDMS stamps was brought to contact the nanoparticle film for 10 s. Then, the PDMS stamp was lifted from the film. Normally, small water drops remained at the edge of the PDMS stamp. A piece of clean soft paper was used to absorb away the water drops, otherwise they wound influence the quality of transferred nanoparticle arrays. Immediately after the inking of a PDMS stamp, conformal printing was performed onto a solid substrate.

Fabrication of devices

To fabricate devices for electronic measurements, we used optical lithograph (SÜSS MicroTec, MJB4) to prepare contract pads with 2 μm inter-distance. Metals (5 nm Ti + 25 nm Au + 50 nm Cr) were e-beam

evaporated for the pads. The Cr layer was used as the inductive coupled plasmon (ICP) etching resist. A second optical lithography was used to define the channel between electrodes and also protected by a layer of Cr (70 nm). ICP etching (TRION) was carried out to etch down the regions that were not protected by Cr layer. Afterwards, the Cr layer was removed by the chromium etchant (Sigma-aldrich).

Molecular exchange

To introduce OPE molecule into the nanoparticle arrays, the as-prepared samples were immersed in the 1mM solution of OPE molecules dissolved in Tetrafuran for more than 12 hours. After that, the samples were taken out and rinsed in tetrafuran for several times and blew dry with nitrogen gas.

Characterization and transport measurements

Nanoparticle arrays and devices are mainly characterized by SEM (FEI Quanta 600). We measured the electronic transport properties of devices with a cryostat (Oxford Ins., OptistatAC-V). The IV curves were measured using a data acquired board (National Instruments, PCI-6281) together with a homemade LabVIEW program. A current amplifier (Keithley 428) was used to convert the current to voltage. The temperature of the devices was controlled by a temperature controller (ITC, Model 503). For nanoparticle arrays with different particle sizes, we measured devices made from nanoparticles with diameters of 6.66 nm (3 devices), 7.58 nm (1 device), 9.25 nm (2 devices), 10.02 nm (3 devices), 10.64 nm (2 devices), 11.09 nm (4 devices), 15.81 nm (2 devices), and 21.35 nm (1 device). For nanoparticle arrays with different ligand molecules, we measured devices made from nanoparticles with ligand molecules of butanethiol (3 devices), hexanethiol (5 devices), octanethiol (4 devices), and decanethiol (4 devices). For nanoparticle arrays changing the dimensionality layer by layer, we measured 3 devices. For nanoparticle arrays with different surrounding molecules, we measured 3 devices.

Acknowledgement. This work was supported by the National Natural Science Foundation of China (No. 60971001), the Ministry of Science and Technology (No. 2011CB933001, 2012CB932702), and the Specialized Research Fund for the Doctoral Program of High Education (No. 20090001120025).

References

[1] Zabet-Khosousi, A.; Dhirani, A.A. Charge transport in nanoparticle assemblies. *Chem. Rev.* **2008**, 108, 4072-4660.

[2] Chang, W.S.; Willingham, B.; Slaughter, L.S.; Dominguez-Medina, S.; Swanglap, P.; Link, S. Radiative and nonradiative properties of single plasmonic nanoparticles and their assemblies. *Acc. Chem. Res.* **2012**, 45, 1936-1945.

[3] Reddy, V.A.; Pathak, N.P.; Nath, R. Particle size dependent magnetic properties and phase transitions in multiferroic $BiFeO_3$ nano-particles. *J. Alloys Compd* **2012**, 543, 206-212.

[4] Nie, Z.; Petukhova, A.; Kumacheva, E. Properties and emerging applications of self-assembled structures made from inorganic nanoparticles. *Nature Nanotech.* **2010**, 5, 15-25.

[5] Talapin, D. V.; Lee, J. S.; Kovalenko, M. V.; Shevchenko, E. V. Prospects of colloidal nanocrystals for electronic and optoelectronic applications. *Chem. Rev.* **2010**, 110, 389-458.

[6] Tang, Z.; Kotov, N.A. One-dimensional assemblies of nanoparticles: Preparation, properties, and promise. *Adv. Mater.* **2005**, 17, 951-962.

[7] Bigioni, T.P.; Lin, X.M.; Nguyen, T.T.; Corwin, E.I.; Witten, T.A.; Jaeger, H.M. Kinetically driven self assembly of highly ordered nanoparticle monolayers. *Nature Mater.* **2006**, 5, 265-270.

[8] Lu, Z.; Yin, Y. Colloidal nanoparticle clusters: functional materials by desigh. *Chem. Soc. Rev.* **2012**, 41, 6874-6887.

[9] Claridge, S. A.; Castleman, A. W.; Khanna, S. N.; Murray, C. B.; Sen, A.; Weiss, P. S. Cluster-assembled materials. *ACS Nano* **2009**, 3, 244-255.

[10] Wang, L.B.; Xu, L.G.; Kuang, H.; Xu, C.L.; Kotov, V.A. Dynamic nanoparticle assemblies. *Acc. Chem. Res.* **2012**, 45, 1916-1926.

[11] Pileni, M.P. Self organization of inorganic nanocrystals: Unexpected chemical and physical properties. *J. Colloid Interface Sci.* **2012**, 388, 1-8.

[12] Chen, J.; Dong, A.; Cai, J.; Ye, X.; Kang, Y.; Kikkawa, J. M.; Murray, C. B. Collective dipolar interactions in self-assembled magnetic binary nanocrystal superlattice membranes. *Nano Lett.* **2010**, 10, 5103-5108.

[13] Kano, S.; Azuma, Y.; Maeda, K.; Tanaka, D.; Sakamoto, M.; Teranishi, T.; Smith, L.W.; Smith, C.G.; Majima, Y. Ideal discrete energy levels in synthesized Au nanoparticles for chemically assembled single-electron transistors. *ACS Nano* **2012**, 6, 9972-9977.

[14] Kane, J.; Ong, J.; Saraf, R.F. Chemistry, physics, and engineering of electrically percolating arrays of nanoparticles: a mini review. *J. Mater. Chem.* **2011**, 21, 16846-16858.

[15] Quinn, A.J.; Beecher, P.; Iacopino, D.; Floyd, L.; Marzi, G.D.; Shevchenko, E.V.; Weller, H.; Redmond, G. Manipulating the charging energy of nanocrystal arrays. *Small* **2005**, 1, 613-618.

[16] Herrmann, J.; Bray, D.J.; Muller, K.-H; Wei, G.; Lindoy, L.F. Tunning the Coulomb charging energy in cross-linked nanoparticle films. *Phys. Rev. B* **2007**, 76, 212201.

[17] Wuelfing, W.P.; Green, S.J.; Pietron, J.J.; Cliffel, D.E.; Murray, R.W. Electronic conductivity of solid-state, mixed-valent, monolayer-protected Au clusters. *J. Am. Chem. Soc.* **2000**, 122, 11465-11472.

[18] Greshnykh, D.; Fromsdorf, A.; Weller, H.; Klinke, C. On the electric conductivity of highly ordered monolayers of monodisperse metal nanoparticles. *Nano Lett.* **2009**, 9, 473-478.

[19] Schmid, G.; Simon, U. Gold nanoparticles: assembly and electrical properties in 1-3 dimensions. *Chem. Comm.* **2005**, 697-701.

[20] Cai, Y.; Wolfkuhler, D.; Myalitsin, A.; Perlich, J.; Meyer, A.; Klinke, C. Tunnable electrical transport through annealed monolayers of monodisperse cobalt-platinum nanoparticles. *ACS Nano* **2011**, 5, 67-72.

[21] Aleksandrovic, V.; Greshnykh, D.; Randjelovic, I.; Fromsdorf, A.; Kornowski, A.; Roth, S.V.; Weller, H. Preparation and electrical properties of Cobalt-Platinum nanoparticle monolayers deposited by the Langmuir-Blodgett technique. *ACS Nano* **2008**, 2, 1123-1130.

[22] Wessels, J.M.; Nothofer, H.G.; Ford, W.E.; Wrochem, F.V.; Scholz, F.; Vossmeyer, T.; Schroedter, A.; Weller, H.; Yasuda, A. Optical and electrical properties of three-dimentional interlinked gold nanoparticle assemblies. *J. Am. Chem. Soc.* **2004**, 126, 3349-3356.

[23] Stansfield, G.L.; Thomas, P.J. Substituent effects on charge transport in films of Au nanocrystals. *J. Am. Chem. Soc.* **2012**, 134, 11888-11891.

[24] Doty, R.C.; Yu, H.; Shih, C.K.; Korgel, B.A. Temperature-dependent electron transport through silver nanocrystal superlattices. *J. Phys. Chem. B* **2001**, 105, 8291-8296.

[25] Ancona, M.G.; kruppa, W.; Rendell, R.W.; Snow, A.W.; Park, D.; Boos, J.B. Coulomb blockade in single-layer Au nanocluster films. *Phys. Rev. B* **2001**, 64, 033408.

[26] Tran, T.B.; Beloborodov, I.S.; Hu, J.; Lin, X.M.; Roserbaum, T.F.; Jaeger, H.M. Sequential tunneling and inelastic cotunneling in nanoparticle arrays. *Phys. Rev. B* **2008**, 78, 075437.

[27] Black, C.T.; Maurray, C.B.; Sandstrom, R.L.; Sun, S. Spin-dependent tunneling in self-assembled Cobalt-nanocrystal superlattices. *Science* **2000**, 290, 1131-1134.

[28] Beecher, P.; Quinn, A.J.; Shevchenko, E.V.; Weller, H.; Redmond, G. Charge transport in weakly coupled $CoPt_3$ nanocrystal assemblies. *J. Phys. Chem. B* **2004**, 108, 9564-9567.

[29] Brust, M.; Bethell, D.; Schiffrin, D.J.; Kiely, C.J. Novel gold-dithiol nano-networks with non-metallic electronic properties. *Adv. Mater.* **1995**, 7, 795-797,

[30] Noguchi, Y.; Terui, T.; Katayama, T.; Matsushita, M.M.; Sugwara, T. Charge transport in various dimensions of small networks composed of gold nanoparticles and terthiphene wire-molecules. *Appl. Phys. Lett.* **2011**, 98, 263114

[31] Huang, S.; Tsutsui, G.; Sakaue, H.; Shingubara, S.; takahagi, T. Well-size-controlled colloidal gold nanoparticles dispersed in organic solvents. *Jpn. J. Appl. Phys.* **2001**, 40, 346-349.

[32] Liao, J.; Li, X.; Wang, Y.; Zhang, C.; Sun, J.; Duan, C; Chen, Q.; Peng, L. Patterned close-packed nanoparticle arrays with controllable dimensions and precise locations. *Small* **2012**, 8, 991-996.

[33] Parthasarathy, R.; Lin, X.M.; Elteto, K.; Rosenbaum, T.F.; Jaeger, H.M. Percolating through networks of random thresholds: Finite temperture electron tunneling in metal nanocrystal arrays. *Phys. Rev. Lett.* **2004**, 92, 076801.

[34] Elteto, K.; Antonyan, E.G.; Nguyen, T.T.; Jaeger, H.M. Model for the onset of transport in systems with distributed thresholds for conduction. *Phys. Rev. B* **2005**, 71, 064206.

[35] Laikhtman, B.; Wolf, E.L. Tunneling time and effective capacitance for single electron tunneling. *Phys. Lett. A* **1989**, 139, 257-260.

[36] Neugebauer, C.A.; Webb, M.B. Electrical conduction mechanism in ultrathin, evaporated metal films. *J. Appl. Phys.* **1962**, 33, 74-82.

[37] Liao, J.; Bernard, L.; Langer, M.; Schonerberger, C.; Calame, M. Reversible formation of molecular junctions in 2D nanoparticle arrays. *Adv. Mater.* **2006**, 18, 2444-2447.

[38] Dayen, J.F.; Devid, E.; Kamalakar, M.V.; Golubev, D.; Guedon, C.; Faramarzi, V.; Doudin, B.; van der Molen, S.J. Enhancing the molecular signature in molecule-nanoparticle networks via inelastic cotunneling. *Adv. Mater.* **2013**, 25, 400-404.

[39] Porter, M.D.; Bright, T.B.; Allara, D.L.; Chidsey, C.E.D. Spontaneously organized molecular assemblies. 4. Structural characterization of n-alkyl thiol monolayers on gold by optical ellipsometry, infrared spectroscopy, and electrochemistry. *J. Am. Chem. Soc.* **1987**, 109, 3559-3568.

[40] Rampi, M.A.; Schueller, O.J.A.; Whitesides, G.M. Alkanethiol self-assembled monolayers as the dielectric of capacitors with nanoscale thickness. *Appl. Phys. Lett.* **1998**, 72, 1781-1783.

[41] Stapleton, J.J.; Harder, P.; Daniel, T.A.; Reinard, M.D.; Yao, Y.; Price, D.W.; Tour, J.M.; Allara, D.L. Self-assembled oligo(phenylene-ethynylene) molecular electronic switch monolayers on gold: structures and chemical stability. *Langmuir* **2003**, 19, 8245-8255.

[42] Tammer, M.; Monkman, A.P. Measurement of the anisotropic refractive indices of spin cast thin poly(2-methoxy-5-(2'-ethyl-hexyloxy)-p-phenylenevinylene)(MEH-PPV) films. *Adv. Mater.* **2002**,

14, 210-212.

[43] Bernard, L.; Kamdzhilov, Y.; Calame, M.; van der Molen, S.J.; Liao, J.; Schönenberger, C. Spectroscopy of molecular junction networks obtained by place exchange in 2D nanoparticle arrays. *J. Phys. Chem. C* **2007**, 111, 18445-184560.

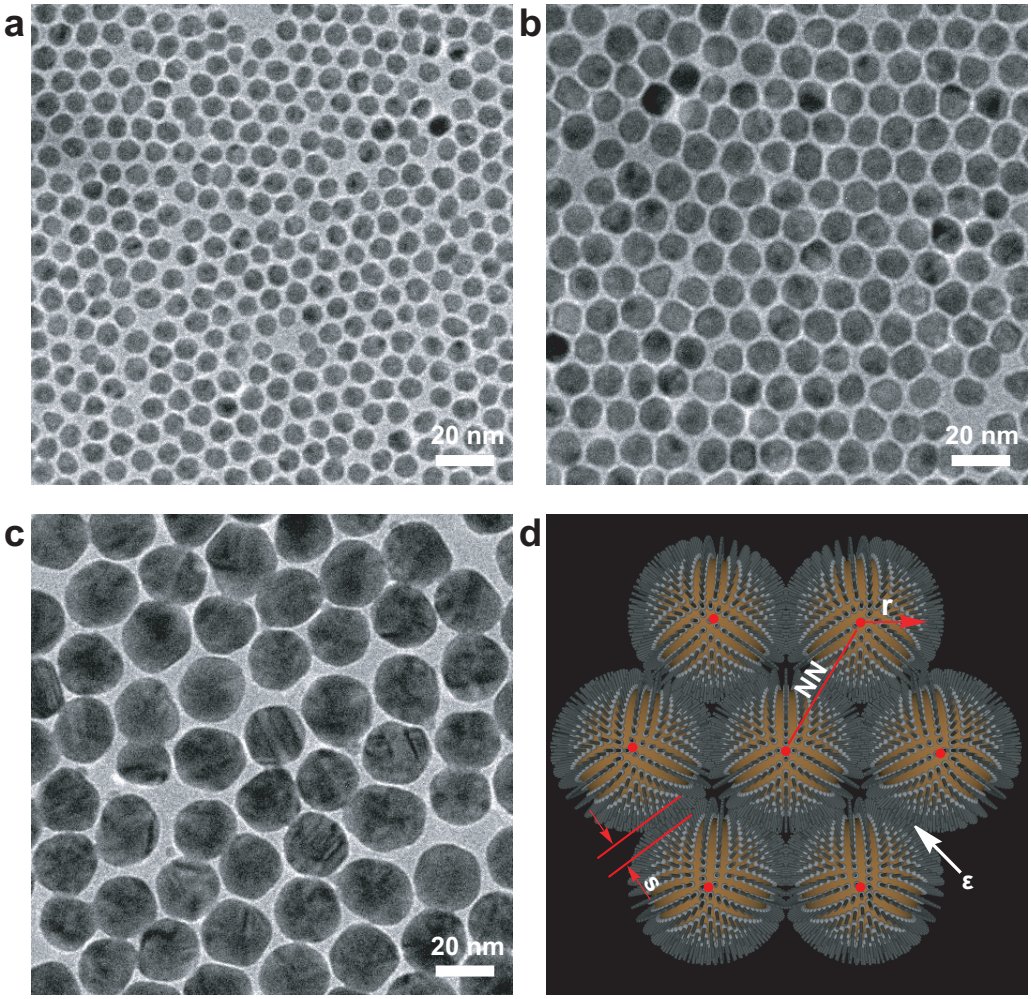

FIG. 1: **Close-packed nanoparticle arrays made from alkanethiol-capped Au nanoparticles. a-c,** Scanning electron microscope images of two-dimensional dodecanethiol-capped Au nanoparticle arrays with different core sizes. The diameter of nanoparticles is 6.66 nm (**a**), 10.02 nm (**b**), and 21.35 nm (**c**). **d,** Schematic of a nanoparticle array, showing the parameters that can be tuned to control the Coulomb charging energy, including the nanoparticle radium **r**, the inter-particle distance **s**, the nearest neighbor number **NNN**, and the dielectric constant of the surrounding molecules ε.

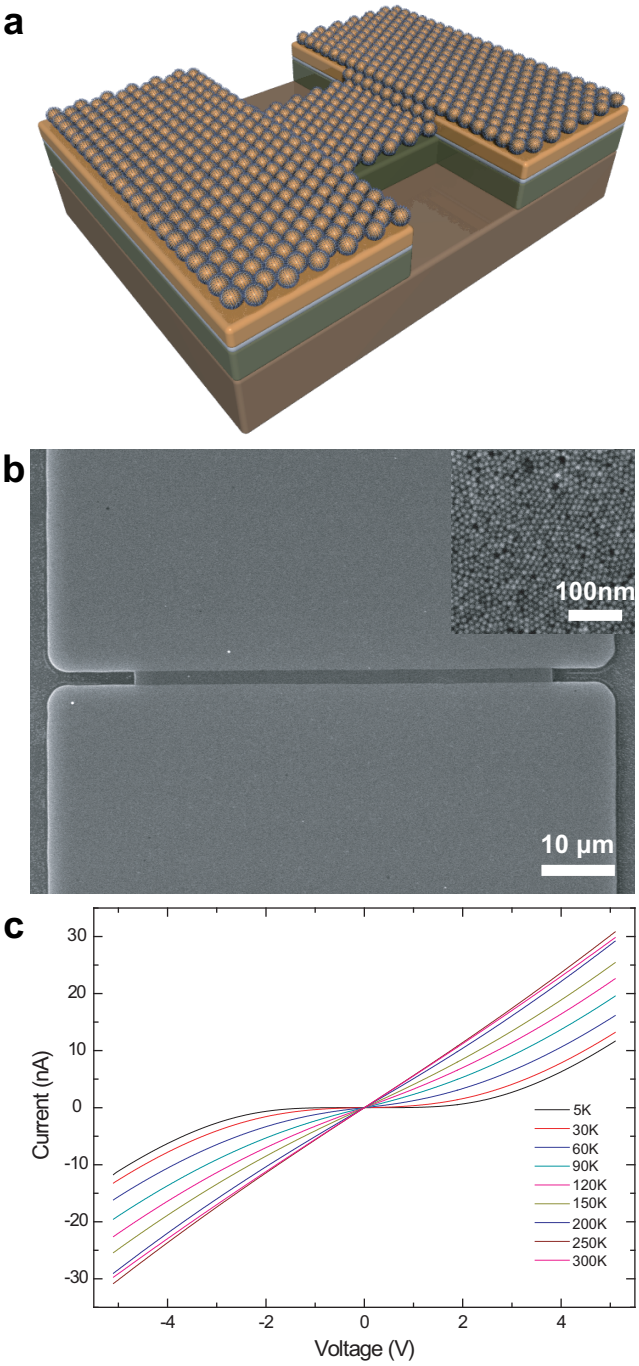

FIG. 2: **Device structure and the general current-voltage curves measured at different temperatures.** **a,** Schematic of the nanoparticle devices. The nanoparticle array between two electrodes (5 nm Ti + 25 nm Au) is well defined by the protrusion region of the substrate. **b,** SEM image of one typical nanoparticle device. The nanoparticle array between two electrodes is 60 μm wide and 2 μm long. Inset: A high magnification SEM image of the nanoparticle array under test. **c,** Current-voltage curves of a typical device measured at different temperatures, ranging from 5 K to 300 K.

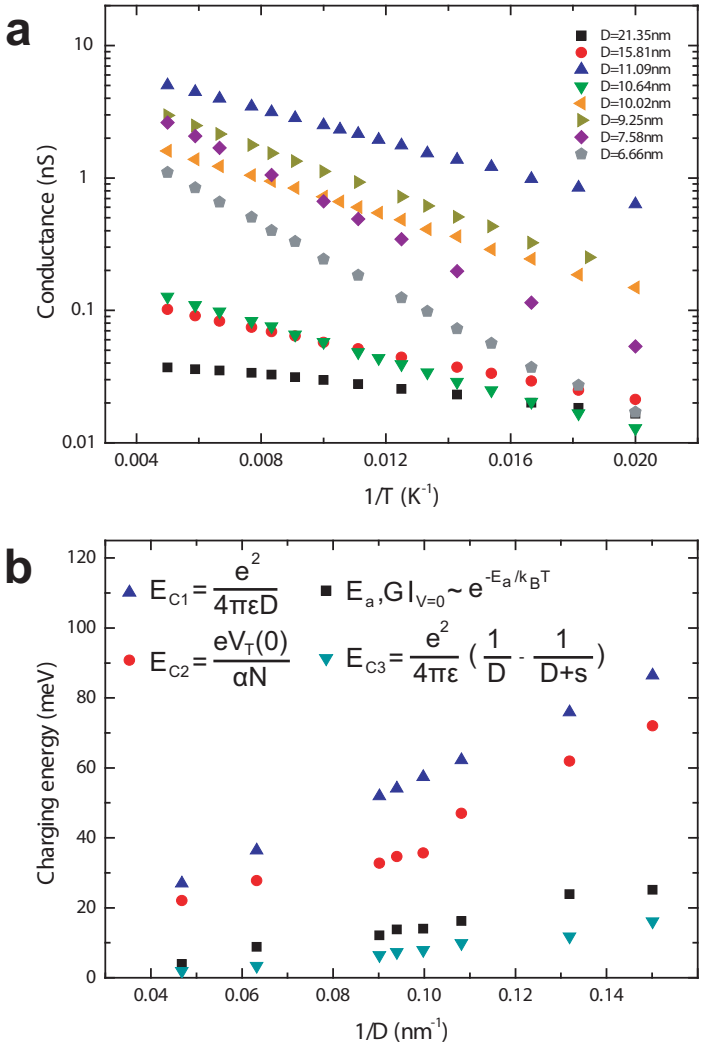

FIG. 3: **The dependence of the Coulomb charging energy of nanoparticle arrays upon the nanoparticle core sizes. a,** The zero-voltage conductance of the nanoparticle arrays as a function of inverse temperature for different nanoparticle core size. Eight different nanoparticle core sizes are measured, from 6.66 nm to 21.35 nm in diameter. Octanethiol molecules were used as ligands for all samples here. **b,** Coulomb charging energy extracted by using four different methods for nanoparticle arrays of different nanoparticle core sizes. Values of Coulomb charging energy obtained from different models are shown by different symbols and different colors: simple isolated nanoparticle model (▲), Arrhenius activation model (■), threshold voltage model (●), and concentric metal model (▼)

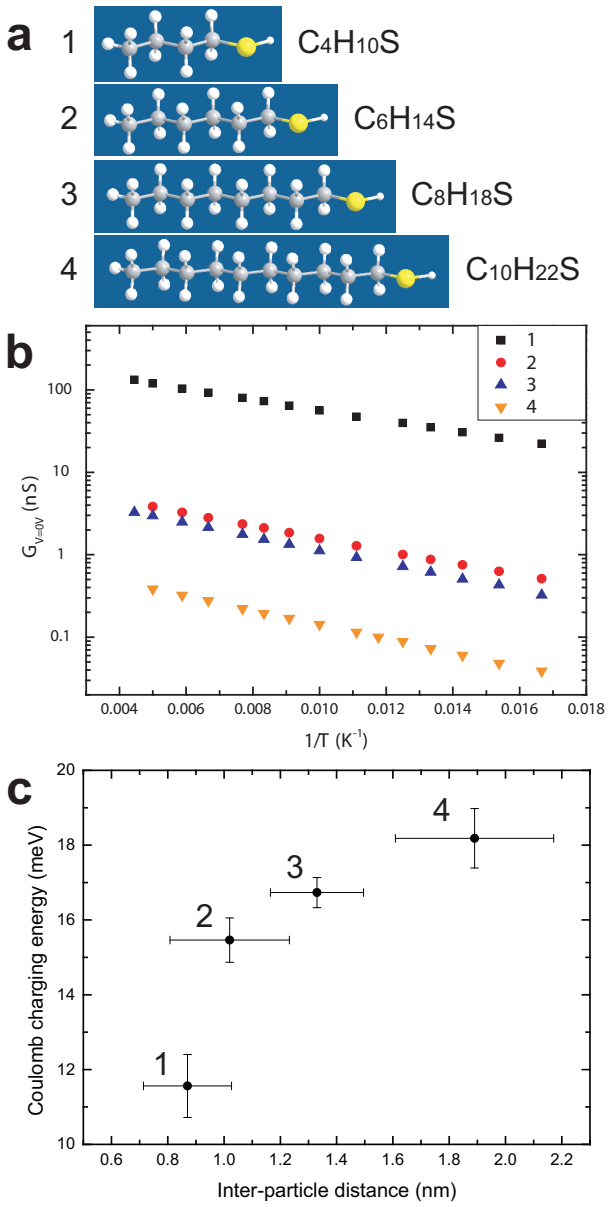

FIG. 4: **The dependence of the Coulomb charging energy of nanoparticle arrays upon the inter-particle distance. a,** Molecular structures of four alkane thiols that are used to encapsulate Au nanoparticles. The length of these alkane thiols are different, leading to different inter-particle distances in nanoparticle arrays. The diameter of gold nanoparticles used here was 9.25 nm. **b,** The zero-voltage conductance of the nanoparticle arrays as a function of inverse temperature for nanoparticle arrays with different inter-particle distances. **c,** The Coulomb charging energy as a function of inter-particle distance.

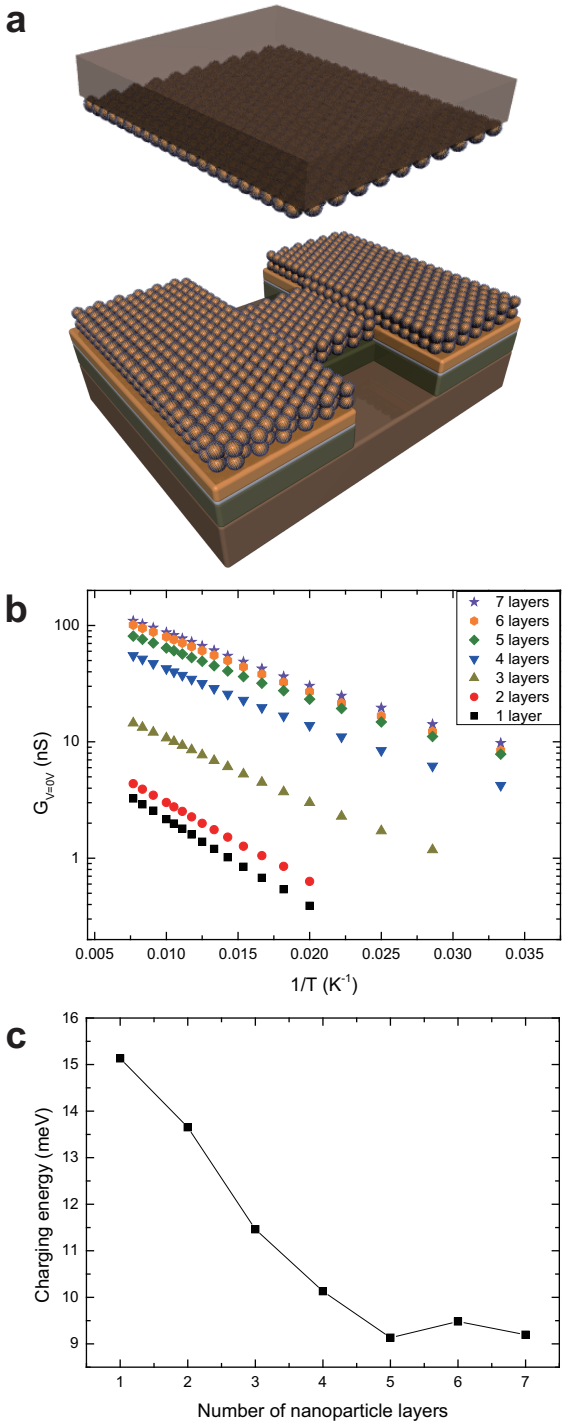

FIG. 5: **The dependence of the Coulomb charging energy upon the dimensionality of nanoparticle arrays. a,** Schematic of the fabrication process to increase the dimensionality of the nanoparticle array under test layer by layer. **b,** The zero-voltage conductance of the nanoparticle arrays as a function of inverse temperature for nanoparticle arrays with different layers, from 1 layer to 7 layers. **c,** The Coulomb charging energy as a function of layers of the nanoparticle array. The diameter of gold nanoparticles used here was 11.09 nm and the liagand molecule was octanethiol.

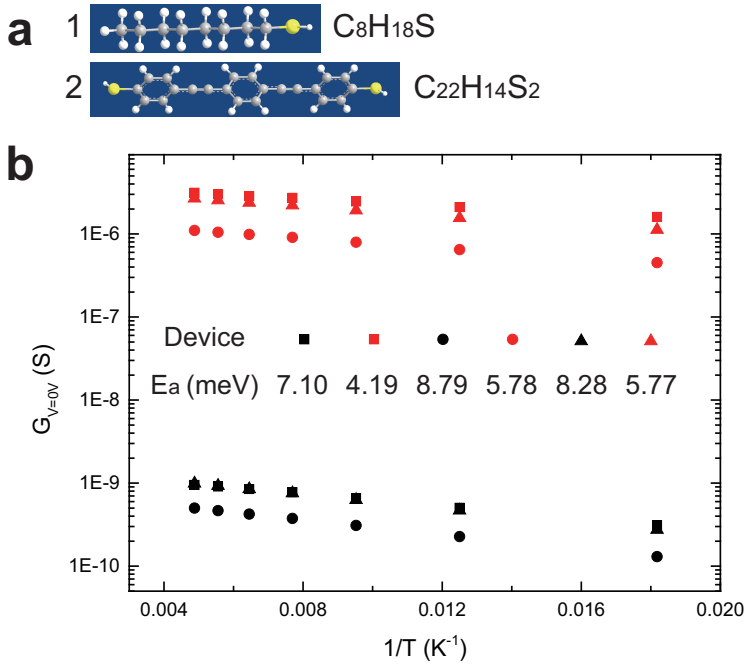

FIG. 6: **The dependence of the Coulomb charging energy of nanoparticle arrays upon the dielectric constant of the surrounding molecules. a,** Molecular structure of two different molecules, which have different dielectric constants. One is octanethiol, and the other is dithiolated oligo(phenylene ethynylene) (OPE). **b,** The zero-voltage conductance of the nanoparticle arrays as a function of inverse temperature for three devices measured before and after OPE molecular exchange. Inset: The Coulomb charging energy for each device measured before(black) and after(blue) molecular exchange. The diameter of gold nanoparticles used here was 10.02 nm.